Original Article

Institution of MECHANICAL ENGINEERS
Journal of POWER AND ENERGY

Proc IMechE Part A:
J Power and Energy
0(0) 1–12

DOI: 10.1177/0957650913487529
pia.sagepub.com
SAGE

Optimization of water jet pumps using numerical simulation

R Yapıcı[1] and K Aldaş[2]

Abstract

A water jet pump is one of the best examples of a device in which liquid-jet mixing phenomena occur. Since such mixing processes are complex, the choice of turbulence model for accurate prediction of performance of the pumps is important. The aim of this numerical simulation study is to investigate effects of parameters such as the jet pump area ratio, nozzle position, and length of the mixing chamber on the pump performance and then to perform an optimization of six different water jet pumps according to these parameters, taking energy efficiency as a criterion. In the optimization procedure, the transition SST model (γ-Re_θ) was used because it provided more accurate results among the four advanced turbulence models. The numerical results obtained with the model were compared with experimental data of the jet pump with the same geometry at the boundary conditions available in the literature and it was seen that maximum deviation in the pump efficiency at the optimum operating conditions was approximately 10%. As a result, the maximum numerical efficiency is found to be 34.6% at the area ratio of 4.61 and a pressure ratio of 0.277.

Keywords

Computational fluid dynamics, water jet pump, optimization, flow simulation, liquid ejector

Date received: 3 November 2012; accepted: 3 March 2013

Introduction

The ***working principle*** of water jet pumps, in other words, the energy conversion process in the pumps, differs from other roto-dynamic (impeller) and positive-displacement pumps due to the absence of moving components. Instead of a rigid working element such as impeller and piston, the pumping process is carried out by transferring energy from a high-pressure fluid to a low-pressure one through friction and momentum transfer. However, this energy exchange between the fluids is highly irreversible; the resulting energy losses cannot be completely eliminated but they can be decreased considerably by selecting the appropriate mass flow ratios and their basic geometrical dimensions based on efficient operating conditions. Although water jet pumps have been used in application fields such as emergency draining, hydraulic dredging, priming of pumps with moving element, the pumping of oil-well production and cooling of nuclear reactors, their optimization or energy efficiency is particularly important in large-scale pumping systems that operate almost continually.

A pressurized liquid functions like a rigid working part and it is required to operate jet pumps. In other words, low-pressured water is pumped by high-pressured water behaving as a driving energy source. Although the water jet pump appears to be simple with respect to its geometry and operation, the negative influence of any error in its design and manufacturing can have a large-scale effect on the efficiency of the pump. Such errors can be determined by analyzing the design of the jet pump using a computational fluid dynamics (CFD) simulation code. The five main components of a water jet pump are suction chamber, suction nozzle, driving nozzle, mixing chamber/tube, and diffuser are shown in Figure 1.

CFD simulation is a lower cost, reliable, and easy to use method in comparison with experimentation; it allows numerous repetitions of the tests requiring a smaller work area, less time, and personnel which makes it a superior simulation technique. This modern technique also provides the possibility of performing modifications in the design with less expense and time, by easily analyzing the flow field or physical details of flow, and achieving an improvement in, and optimization of the design. Due to its outstanding

[1]Department of Mechanical Engineering, Faculty of Engineering, Selçuk University, Konya, Turkey
[2]Department of Mechanical Engineering, Faculty of Engineering, Aksaray University, Aksaray, Turkey

Corresponding author:
R Yapıcı, Department of Mechanical Engineering, Selçuk University, Alaeddin Campus, 42250 Konya, Turkey.
Email: rafet@selcuk.edu.tr

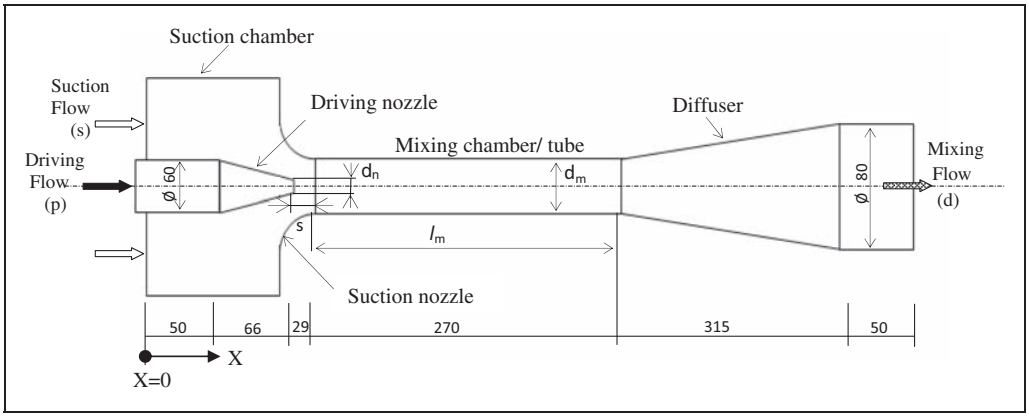

Figure 1. Schematic of the computational domain.

performance, the CFD technique has begun to be widely used by engineers and researchers in estimating the flow field within jet pumps. In the literature, there are a large number of studies analyzing jet pumps using this numerical technique. The primary and secondary fluids used in these studies are fluid pairs such as liquid–liquid,[1–4] gas–liquid,[5–8] and gas–gas.[9–12]

In the study by Winoto et al.,[13] the effects of the driving nozzle type on the performance of water jet pumps were investigated using a one-dimensional theory and experimentation; consequently, the best efficiency in this work was obtained with a circular nozzle.

Prakeao et al.[1] numerically analyzed the flow field within a water jet pump using a three-dimensional RNG k-ε turbulence model. This numerical study ***focused on the*** determination of the optimum geometrical parameters including the area ratio, nozzle position, and mixing tube length. Neto and Porto[14] compared the efficiencies of Venturi-type ejectors with those of low-cost ejectors developed as an outcome of the tests which were carried out with the various area ratios. According to their experimental and theoretical results, the developed ejector had an efficiency that was double and triple of that of other ejectors. They achieved an ejector design with the best efficiency at an area ratio of 2.85. The authors recommended that the flow ratio should not exceed an area ratio of 2 for an efficient pumping without flow separation and cavitations.

Henzler[15] discussed a theoretical design model, which included empirical adaptation parameters, for single-phase ejectors. Since the results of the model were in agreement with the experimental data in the literature, an ejector geometry with a constant-area mixing tube was proposed based on both the data and the model results. Hammoud[16] experimentally investigated the performances of a water jet pump for two different suction configurations. In his work, the efficiency and pressure ratio of the pump were determined in terms of flow ratio. According to the results, when compared with the down-feeding configuration, the up-feeding configuration has a higher pressure ratio but lowers the jet pump efficiency. Hayek and Hammoud[2] estimated the efficiency of a water jet pump as a function of the mass flow ratio using different turbulence models. Long et al.[3] investigated the effects of exit tip thickness of the driving nozzle on the performance of a water jet pump using the standard k-ε turbulence model and the efficiency of a jet pump with an area ratio of 6.27 was found to be 34.9% at a flow ratio of 2.

Karambirov and Chebaevskii[17] presented the generalized dimensional characteristics for the optimum design of ejector (jet) pumps. To increase efficiencies of these pumps, they recommended that improving the mode of entry of the suction fluid to the pump and the use of the stepped diffuser. According to the generalized jet pump characteristics generated by the researchers, a pump efficiency of 42% can be achieved with a substantially improved design. Yapıcı[18] performed a theoretical and experimental study to determine the optimum operating conditions of water jet pumps. The one-dimensional theoretical model overestimated the efficiency and pressure ratio of the jet pump compared to experiments undertaken using intermediate-size jet pumps. One of the most comprehensive theoretical and experimental studies on the water jet pumps was carried out by Schulz and Fasol.[19] In the experimental study using a large-size water jet pump ($d_m = 101$ mm), the maximum value of the jet pump efficiency obtained at the flow ratio 1.07 and the area ratio 3.56 was 37%, while the pressure ratio was around 0.345. Such a high efficiency was achieved by optimizing all the flow and geometrical parameters. Moreover, in order to improve the efficiency of the water jet pump that was tested, the tubes orienting the suction (secondary) flow were located at the front of suction chamber so that suction flow enters into the chamber ***homogeneously*** and axisymmetrically. Narabayashi et al.[4] examined a water jet pump with an area ratio of 4 experimentally and numerically. The results using the standard k-ε turbulence model showed that a peak efficiency of 36% was reached at a flow ratio of 1.3.

El Gazzar et al.[20,21] investigated experimentally and numerically the effect of adding drag reduction

agents to secondary stream on the performance of water jet pumps. They carried out their tests using carboxy methyl cellulose (CMC) as an additional agent. The authors concluded in their experimental study that the overall efficiency of the pump increased up to a certain value of CMC concentration. Moreover, the researchers made a comparison between the experimental and numerical results and determined that at optimum condition of the concentration, the numerical efficiency is higher than the experimental efficiency by around 10%.

The efficiency of the water jet pumps is at a low level in comparison with other pumps, and their efficiencies are extremely affected by the flow rate ratio especially in the lower area ratios. These two factors further increase the importance of the need for their optimization. The main purpose of this numerical study was to perform the optimization of six different jet pumps using CFD simulation and to assess the validity of the simulation by comparing the CFD results with the optimized experimental results in the literature. By means of these optimization and validation studies, it will be researched whether the CFD technique can be used in the prediction of performances of water jet pumps with a satisfactory accuracy. It appears that there is no published work concerning an optimization study on water jet pumps using CFD techniques over a large range area ratio and validated with experimental data; therefore, the current numerical study will fill this gap in the literature.

CFD modeling

To model the turbulence flow in a water jet pump in CFD simulations, initially four different turbulence models were chosen; the realizable k-ε, SST k-ω, RSM, and transition SST model. The reason for the selection is that they have been extensively validated for a wide range of flows including complex flows such as jets and mixing layer, channel and boundary layer flows, transition and separated flows. Generally, they predict the spreading rate for axisymmetric (round) jets in a sufficient accuracy.[22] The flow within a water jet pump is a combination of flows for which there is a very complex ***underlying physics***. In analyzing the water jet pump using CFD, the following assumptions are made: (i) the flow within the jet pump is steady and incompressible; both the motive and suction (entrained) fluid is water, (ii) the heat transfer between water and surroundings does not exist, (iii) the surface roughness is taken as zero, and (iv) the effect of buoyancy is ignored.

Based on these assumptions, the continuity and momentum equations can be written as

$$\frac{\partial \rho u_i}{\partial x_i} = 0 \tag{1}$$

$$\frac{\partial}{\partial x_j}(\rho u_j u_i) = \frac{\partial}{\partial x_j}\left[\mu \frac{\partial u_i}{\partial x_j} - \rho \overline{u_i u_j}\right] - \frac{\partial p}{\partial x_i} \tag{2}$$

where the Reynolds stresses are

$$-\rho \overline{u_i u_j} = \mu_t \left[\frac{\partial u_i}{\partial x_j} + \frac{\partial u_j}{\partial x_i}\right] - \frac{2}{3}\rho k \delta_{ij} \tag{3}$$

The transition SST model is based on the coupling of the original SST model with another two transport equation; the Local Correlation Based Transition (LCTM or γ-Re_θ) Model. In the γ-Re_θ model, γ is the intermittency equation and the value of the turbulence intermittency shows whether a given point is located inside the turbulent region and also the local effect of the turbulence intensity is taken into consideration through this equation. The transitional momentum-thickness Reynolds number Re_θ is an important local property which indicates the transition onset criteria and includes non-local effect of the turbulence intensity. The four-equation model is capable of capturing the transition from laminar to turbulent flow and vice versa. This model has been developed by Langtry and Menter[23,24] in order to cover the transition between these flows.

Details for the four model equations belong to the transition SST model used in this optimization study are given below. In the model, production and destruction terms of the original SST model are modified using the intermittency and the model combines the experimental correlations with locally formulated γ-Re_θ equations. The transport equation for the intermittency γ is

$$\frac{\partial(\rho\gamma)}{\partial t} + \frac{\partial(\rho U_j \gamma)}{\partial t_j} = P_{\gamma 1} - E_{\gamma 1} + P_{\gamma 2} - E_{\gamma 2} + \frac{\partial}{\partial x_j}\left[\left(\mu + \frac{\mu_t}{\sigma_\gamma}\right)\frac{\partial \gamma}{\partial x_j}\right] \tag{4}$$

The transition source terms are given by

$$P_{\gamma 1} = C_{a1} F_{length} \rho S[\gamma F_{onset}]; \quad E_{\gamma 1} = C_{e1} P_{\gamma 1} \gamma \tag{5a - b}$$

The source terms for the destruction/relaminarzation are defined as

$$P_{\gamma 2} = C_{a2} \rho \Omega S \gamma F_{turb}; \quad E_{\gamma 2} = C_{e2} P_{\gamma 2} \gamma \tag{6a - b}$$

The transition onset is controlled by the following functions

$$\mathrm{Re}_V = \frac{\rho y^2 S}{\mu}; \quad \mathrm{R}_T = \frac{\rho k}{\mu \omega} \tag{7a - b}$$

$$F_{onset1} = \frac{\mathrm{Re}_V}{2.193 \mathrm{Re}_{\theta c}};$$
$$F_{onset2} = \min\left(\max\left(F_{onset1}, F_{onset1}^4\right),\ 2.0\right) \tag{8a - b}$$

$$F_{onset3} = \max\left(1 - \left(\frac{\mathrm{R}_T}{2.5}\right)^3, 0\right);$$

$$F_{onset} = \max\left(F_{onset2} - F_{onset3}, 0\right); \quad F_{turb} = e^{-\left(\frac{R_T}{4}\right)^4} \tag{9a - c}$$

$Re_{\theta c}$ is the critical Reynolds number where the intermittency first starts to increase in the boundary layer. F_{length} is an empirical correlation that controls the length of the transition zone. These correlations are functions of $\tilde{R}e_{\theta t}$. The constants for the intermittency equation are $C_{a1} = 2$; $C_{e2} = 1$; $C_{e2} = 50$; $C_{a\gamma} = 0.5$; $C_{\gamma} = 1.0$.

The transition model includes a modification for separation-inducted transition as the following

$$\gamma_{sep} = \min\left(C_{s1}\max\left[\left(\frac{\mathrm{Re}_V}{3.235\mathrm{Re}_{\theta c}}\right) - 1, 0\right]F_{reattch}, 2\right)F_{\theta t};$$

$$F_{reattch} = e^{-\left(\frac{R_T}{20}\right)^4}; \ \gamma_{eff} = \max\left(\gamma, \gamma_{sep}\right) \tag{10a - c}$$

The transport equation for the transition momentum thickness Reynolds number $\tilde{R}e_{\theta t}$ is

$$\frac{\partial\left(\rho\tilde{R}e_{\theta t}\right)}{\partial t} + \frac{\partial\left(\rho U_j\tilde{R}e_{\theta t}\right)}{\partial x_j} = P_{\theta t} + \frac{\partial}{\partial x_j}\left[\sigma_{\theta t}(\mu + \mu_t)\frac{\partial\tilde{R}e_{\theta t}}{\partial x_j}\right] \tag{11}$$

$\tilde{R}e_{\theta t}$ equation allows a connection between the empirical correlations and the onset of transition criterion of the γ equation. The source term for the equation is given by

$$P_{\theta t} = c_{\theta t}\frac{\rho}{t}\left(Re_{\theta t} - \tilde{R}e_{\theta t}\right)(1.0 - F_{\theta t}); \ t = \frac{500\mu}{\rho U^2} \tag{12a - b}$$

$Re_{\theta t}$is the third empirical correlation of the model and it represents the onset of transition determined in experiments. The model constants for $\tilde{R}e_{\theta t}$ equations are $c_{\theta t} = 0.5$ *and* $\sigma_{\theta t} = 1.0$. The empirical correlation is a function of the local turbulence intensity (T_i) and the Thwaites' pressure gradient coefficient (λ_θ) defined as follows

$$\lambda_\theta = \left(\theta^2/\nu\right)\mathrm{d}U/ds \tag{13}$$

where dU/ds is the acceleration in the streamwise direction.

The $F_{\theta t}$ blending function is defined as follows

$$F_{\theta t} = \min\left(\max\left(F_{wake}e^{\left(-\frac{y}{\delta}\right)^4}, 1.0 - \left(\frac{\gamma - 1/50}{1 - 1/50}\right)^2\right), 1.0\right) \tag{14}$$

$$\theta_{BL} = \frac{\tilde{R}e_{\theta t}\mu}{\rho U}; \ \delta_{BL} = \frac{15}{2}\theta_{BL}; \ \delta = \frac{50\Omega y}{U}\delta_{BL} \tag{15}$$

$$\mathrm{Re}_\omega = \frac{\rho\omega y^2}{\mu}; \ F_{wake} = e^{-\left(\frac{\mathrm{Re}_\omega}{1E+5}\right)^2} \tag{16}$$

The transition model is coupled with the SST turbulence model by means of the following equations

$$\frac{\partial}{\partial x_j}\left(\rho u_j k\right) = \tilde{P}_k - \tilde{D}_k + \frac{\partial}{\partial x_j}\left[(\mu + \sigma_k\mu_t)\frac{\partial k}{\partial x_j}\right] \tag{17}$$

$$\tilde{G}_k = \gamma_{eff}P_k; \ \tilde{D}_k = \min\left(\max\left(\gamma_{eff}, 0.1\right), 1.0\right)D_k \tag{18}$$

$$\frac{\partial}{\partial x_j}\left(\rho u_j\omega\right) = \alpha\frac{P_k}{\nu_t} - D_\omega + Cd_\omega + \frac{\partial}{\partial x_j}\left[(\mu + \sigma_k\mu_t)\frac{\partial\omega}{\partial x_j}\right] \tag{19}$$

where P_k and D_k are the original production and destruction terms for the SST turbulence model. The effective intermittency γ_{eff} is used to control the source terms in the equation (17).

In the present modeling study, the drawings of all the jet pumps were drawn in the ANSYS Design Modeler according to the sizes given in the literature,[18] since our numerical results would be compared with the experimental data from Yapıcı.[18] Thus, the geometry of water jet pump used in the CFD simulation is same as the experimental jet pump. The grid in appropriate type (unstructured hybrid cell) and number was generated in the ANSYS Meshing and also was utilized from the adaptive meshing capability of this CFD code. All flow simulations for the water jet pump were performed by the ANSYS Fluent R14.0 CFD code which uses the finite volume method as a numerical solution technique. In order to achieve a more accurate definition of the turbulent flow, the three-dimensional geometry model was used in this study and the computational domain was reduced by half using a symmetry plane to decrease the calculation time and the mesh number. To obtain the mesh-independent solution, the adaptive meshing method was applied and maximum number of cells for a half volume of water within jet pump was around 300,000. Results of grid sensitivity analysis for optimum operating conditions are given in Table 1. Total pressure inlet boundary conditions were used for the motive and entrained flows (p_{tp}, p_{ts}) and static pressure outlet boundary conditions for the mixed (exit) flow (P_d) were implemented to define the flow domain. In the problem setup, the values of these boundary conditions were entered as in the measurement readings (measured inlet and outlet values) given in Ref. 18 and then the mass flow rates of motive, entrained, and mixed flows were computed using the coupled solution algorithm for pressure-velocity coupling, the quick scheme for spatial

Table 1. Sensitivity analysis based on the mass flow ratio for different area ratios (number of cells, NC).

$A=2.05$		$A=3.60$		$A=4.61$		$A=5.92$		$A=7.94$		$A=16.44$	
NC	M	NC	M	NC	M	NC	M	NC	M	NC	M
88,397	0.38	139,855	1.00	130,242	1.22	113,363	1.62	94,444	2.01	108,814	4.11
307,444	0.37	307,075	1.00	312,263	1.25	315,284	1.60	30,1329	2.03	349,758	4.17
493,197	0.38	479,880	1.01	483,231	1.24	617,521	1.60	78,7837	2.01	478,432	4.14

Table 2. Sensitivity analysis based on the mass flow ratio for different area ratios (convergence criteria, CC).

CC	$A=16.44$	$A=7.95$	$A=5.92$	$A=4.61$	$A=3.60$	$A=2.04$
10^{-3}	4.18	2.00	1.60	1.26	0.93	0.36
10^{-4}	4.17	2.03	1.60	1.25	1.00	0.37
10^{-5}	4.24	2.00	1.61	1.26	0.99	0.35

discretization, and the pressure-based solver. The convergence criteria for continuity, momentum, and transport (model) equations were always less than 10^{-4} and iterations were continued until ***the convergence criteria were satisfied.*** Results of sensitivity analysis of the iterative convergence criteria for optimum operating conditions are given in Table 2.

Results and discussion

The operating mode of a water jet pump with a given area ratio does not depend on the absolute values of the pressures and mass flow rates at the inlet and outlet of the pump.[18,19] On the contrary, the dimensionless parameters defined as follows characterize the operating mode of the pump.

Pressure (head) ratio

$$P = \frac{(p_{td} - p_{ts})}{p_{tp} - p_{td})} \tag{20}$$

Mass flow ratio;

$$M = \frac{\dot{m}_s}{\dot{m}_p} \tag{21}$$

These dimensionless quantities determine the energy efficiency of liquid jet pumps

$$\eta = M \times P \tag{22}$$

In the first stage of the comparative study, the numerical mass flow ratios were computed using the realizable k-ε, RSM, SST k-ω, and transition SST models, then the numerical results were compared with experimental flow ratios in the literature. As shown in Figure 2, the transition SST model provides slightly more accurate results than the other turbulence models at a near optimum point ($1.0 < M_{opt} < 1.5$) with the area ratio of 4.61.

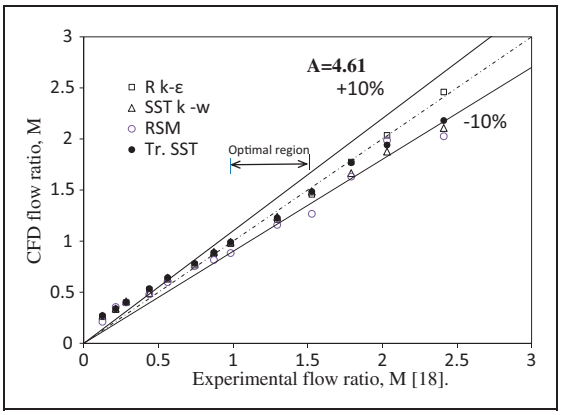

Figure 2. CFD results versus experimental flow ratios.

In the next stage of the study, the performance curves $\eta = f(M)$ and $P = f(M)$ for a given water jet pump with a constant area ratio (A) were generated using the transition SST model and the numerical results were compared with experimental results in Ref. 18. The effects of the main (major) relative geometrical parameters on the pump efficiency were then numerically investigated depending on the mass flow ratio (M). The parameters are the relative length of mixing chamber (L), the relative position of driving nozzle (S), and the area ratio of the jet pump (A). The efficiency of the water jet pump is taken as the criterion in the numerical study of the optimization and the optimum values of the parameters were found. In the final stage of the study, the optimized CFD results for six area ratios were determined and compared with the experimental results, obtained from the same operating conditions, given in the literature.

The performance of a water jet pump for constant area ratio

Both the numerical and experimental performance curves of a water jet pump are shown in Figure 3.

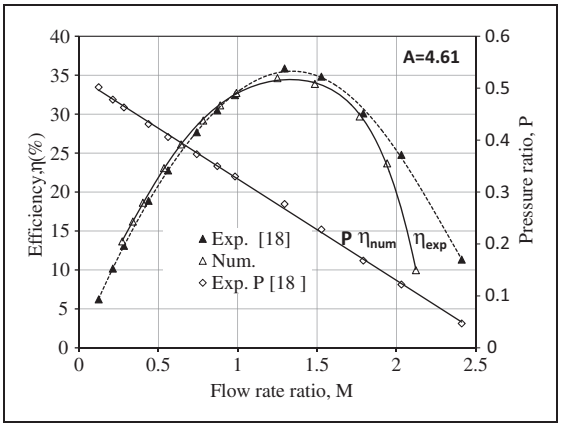

Figure 3. The numerical and experimental performance curves at constant area ratio.

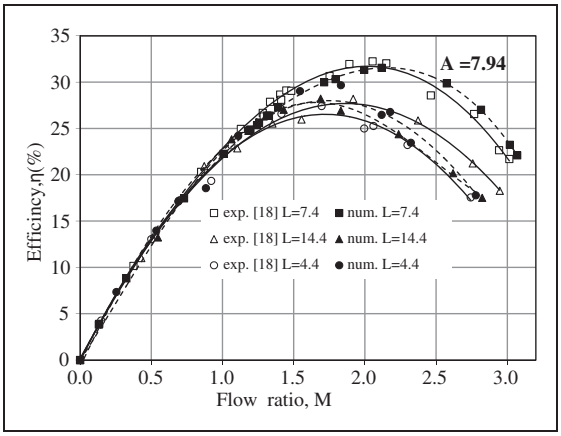

Figure 4. Effect of the mixing chamber length on the efficiency.

It can be clearly seen that the pressure ratio for each test point is same due to the fact that the values of pressures are equal in both the numerical and experimental tests; however, the mass flow ratio is slightly different and this has an impact on the efficiency of the pump.

According to these results, the pressure/head ratio decreased almost linearly with the increase of the mass flow ratio. Since the flow rate of the suction fluid increased with the increasing mass flow ratio, the water pressure at the outlet of the jet pump decreased. The energy of the motive fluid is transferred to the water in higher amounts and this led to a decrease in the pressure ratio. First, the efficiency of the pump increased and then decreased after reaching a maximum value as the mass flow ratio increases. The numerical efficiency results were generally in a very good agreement with experimental results. However, the agreement was not very good in the higher mass flow ratios ($M > 1.7$) compared with the optimum mass flow ratio in which the efficiency was at a peak value. According to the numerical and experimental results at the optimum points for the area ratio $A = 4.61$, the mass flow ratios were $M_{exp} = 1.29$ and $M_{num} = 1.24$, the pressure ratios were $P_{num} = P_{exp} = 0.277$, and the efficiencies were $\eta_{num} = 34.6\%$ and $\eta_{exp} = 35.8\%$. The deviation in numerical efficiency relative to experimental efficiency at the optimum pressure ratio was around 3.4%. The optimized efficiency of water jet pump determined by Schulz and Fasol[19] in their experimental work was $\eta \cong 36\%$ at $M \cong 1.4$ and $P \cong 0.25$ for $A \cong 4.6$. However, they used a large size jet pump in the work with the diameter of the mixing chamber being approximately triple the diameter of the jet pump analyzed in the present study.

A complete explanation for the variations in the initial increase and then decrease with M in the jet pump efficiency can only be given by a detailed examination of the internal structure of flow through its channels. The first interpretation that comes to mind is that the low level of efficiency for $M < M_{,opt}$ can be attributed to sucking smaller amount of fluid (or in lower suction flow rate) because of the low vacuum at the driving nozzle exit and the flow separations at the mixing chamber inlet. The low level of efficiency for $M > M_{,opt}$ can be attributed to the increase of head (energy) losses due to a higher turbulent intensity and even that cavitation can be expected to form in much higher flow ratios.

A comprehensive and understandable explanation of all analysis results can be performed based on the turbulence properties such as turbulent intensity, turbulent kinetic energy, turbulent dissipation rate, and visual results dealing with flow field. The visual results can be obtained by using the ***flow visualization techniques or CFD display methods.***

Effects of geometrical parameters on the performance of jet pump

Effect of the length of the mixing chamber. In order to investigate the effect of the mixing chamber length on the efficiency of water jet pump, three mixing chambers/tubes in lengths of 160, 270, and 525 mm were selected in the current study. The relative length of the mixing chamber L is defined as the ratio of its length to its diameter, l_m/d_m. Based on numerical and experimental data, Figure 4 shows how the length of the mixing chamber affects the water jet pump efficiency as the mass flow ratio increases from 0 to around 3 for the area ratio $A = 7.94$; thus, the CFD results are in good agreement with experimental results over the entire range of the flow ratios. As seen from Figure 4, for both the numerical and experimental studies, the efficiency η becomes a maximum with a value of around 31.3% at $M = 1.99$ for the given area ratio while L is 7.4. Using longer or shorter lengths, this relative length results in a drop in efficiency. The maximum efficiencies for the shorter relative length $L = 4.4$ and the longer relative length $L = 14.4$ were $\eta \cong 29.6\%$ at $M = 1.83$ and $\eta = 26.9\%$ at $M \cong 1.83$, respectively. Accordingly, the optimum relative length of mixing

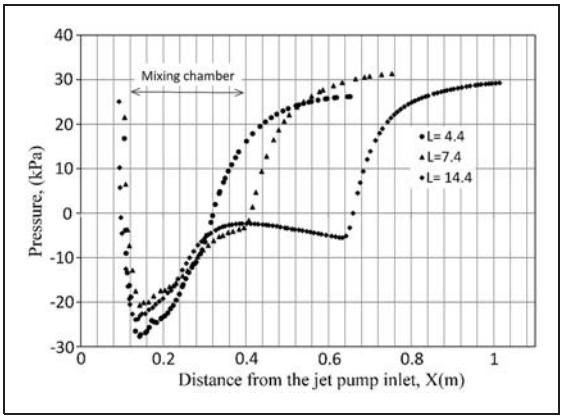

Figure 5. Pressure variations on the jet pump centerline.

chamber is $L = 7.4$ for $A = 7.94$. For the efficiency in the optimum case, the decrease in percentage of the maximum efficiencies for the shorter and longer relative lengths is 5.3% and 14.5%, respectively. According to the experimental data from a number of researchers reported in the literature,[15] this relative length first arises from 1 at $A = 1.3$ to around 7 at $A = 2.5$ and it then remains between 7 and 8 for $A > 2.5$.

The optimum mixing chamber is the length at which momentum transfer between primary and secondary fluids was just completed and also the change of the flow velocity profile ended. Also, the pressure in the chamber reaches its maximum value at the point which corresponds to the optimum length. To determine the velocity distributions at various flow cross-sections along the mixing chamber and the pressure variation on its centerline, the simulation results were re-evaluated. As shown in Figure 5 in the curve for $L = 14.4$, the maximum pressure location is around $X = 0.41$ m, where the relative length is $L \cong 7.4$.

The velocity profiles are generated in the optimum flow ratios corresponding to the three relative chamber lengths and the profiles are displayed in Figure 6. It can be seen from the velocity profiles in Figure 6(a) that the velocity profile continuously changes up to about $L = 8.2$ ($l_7 = 300$ mm); however, it does not vary until it reaches the inlet of the diffuser ($l_{11} = 525$ mm) from this position. This shows that the mixing process completed at approximately the specified distance or length. It is clear that the energy (pressure) losses in the remaining section of the mixing chamber ($l_m - l_{m,opt}$) led to a decrease in the efficiency of the water jet pump. A careful examination of Figure 6(b) shows that the velocity profile tends to remain unchanged toward the end of mixing chamber. This validates the result belonging to $L = 7.4$ as shown in Figure 5.

According to Figure 6(c), the velocity profile always changes throughout the mixing chamber having a relative length of $L = 4.4$ and so the fluids enter the diffuser (the distance of its inlet position being around 0.4 m, $l_5 = 160$ mm) with a higher peak

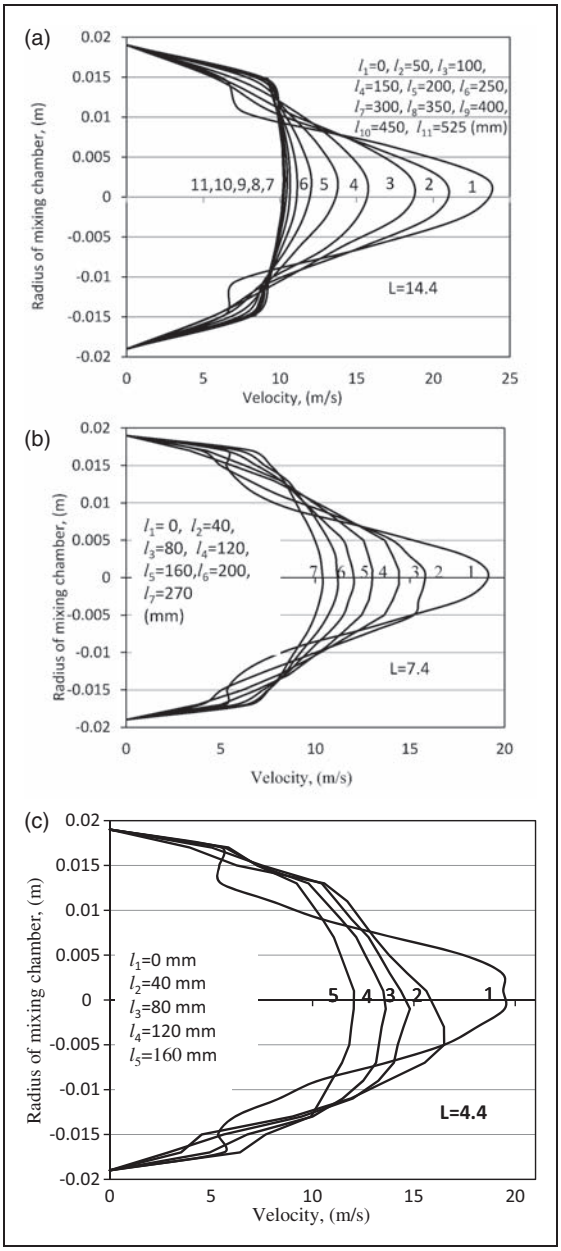

Figure 6. Velocity profiles of flow within the mixing chamber: (a) $L = 14.4$, (b) $L = 7.4$, and (c) $L = 4.4$.

velocity in comparison with other relative lengths without completing the mixing process. This can be clearly seen in Figure 6(c).

Moreover, the volume-averaged turbulence intensity has a minimum value of 2.3% if the jet pump with a relative mixing chamber length of $L = 7.4$ is used; however, the turbulence intensity for other relative lengths such as $L = 4.4$ and $L = 14.4$ are 25% and 32%, respectively. Considering these three results above, the highest efficiency was reached at the relative length $L = 7.4$, which allows just enough length for complete mixing. Then this is the optimum relative length of the mixing chamber.

Effect of the driving nozzle position. The driving nozzle distance, s, is the length between the exit end of the

nozzle and the inlet of mixing tube as shown in Figure 1. The relative position of the nozzle (S) is the ratio of this distance (s) to the diameter of the mixing chamber (d_m), namely $S = s/d_m$. Based on the numerical and experimental data for three relative positions, the effect of the driving nozzle distance on the efficiency of the water jet pump is shown in Figure 7.

In the water jet pumps with constant-area mixing chamber, the driving nozzle is located within suction nozzle before the mixing chamber inlet, so that the entrained liquid can enter the mixing chamber without impinging on the driving nozzle tip and suction nozzle. The distance must be an ***appropriate*** length to not allow the spreading of the driving fluid jet; otherwise, the annular flow section for the entrained (secondary) fluid between the primary jet and the wall of the mixing chamber will be reduced. The numerical solutions for three different position of the nozzle at the area ratio $A = 7.94$ are shown together with experimental results in Figure 7. According to this figure, the lowest efficiency corresponds to the smallest relative nozzle position of $S = 0.44$. The highest jet pump efficiency is attained at $S = 0.74$ and the value is 31.3%. The efficiency of the jet pump decreases due to the increasing energy losses in the suction nozzle for the smaller S values; in other words, when approaching the nozzle towards the mixing chamber. At higher S values, primary jet spreads out before entering the mixing chamber and this spreading causes less fluid to be sucked from suction chamber, thus decreasing the pump efficiency.

It can also be seen from Figure 7 that the agreement between numerical and experimental data for this optimum relative nozzle position is better than those of the other nozzle positions and there is also a good agreement between the results at both the lower and higher flow rate ratios. As seen in Figure 8, the maximum dissipation rates of the turbulent kinetic energy for the nozzle positions $S = 0.44$, $S = 0.74$, and $S = 0.89$ are 2314, 1173, and 1286 m^2/s^3, respectively, and the highest efficiency is obtained at nozzle position $S = 0.74$, at which the energy dissipation rate is at a minimum.

Effect of the area ratio. Figure 9 shows the efficiency curves calculated numerically for six area ratios depending on the flow ratio. The mass flow rate ratio, at which efficiency reaches a maximum, differs for each area ratio and this flow rate ratio corresponds to higher values as the area ratio increases. The numerical solutions here were conducted using the optimum mixing chamber lengths and the optimum driving nozzle positions which were determined numerically and also validated with experimental data given in Ref. 18. The numerical tests are undertaken using water in the range of $1.5 \times 10^4 < (Re = \rho V_m d_m/\mu) < 4 \times 10^5$ and the test range matched the experimental range referenced for comparison.

A demonstratively important result in the Figure 9 is that the efficiency is more sensitive to the flow ratio changes in the lower area ratios. Also, a lower area

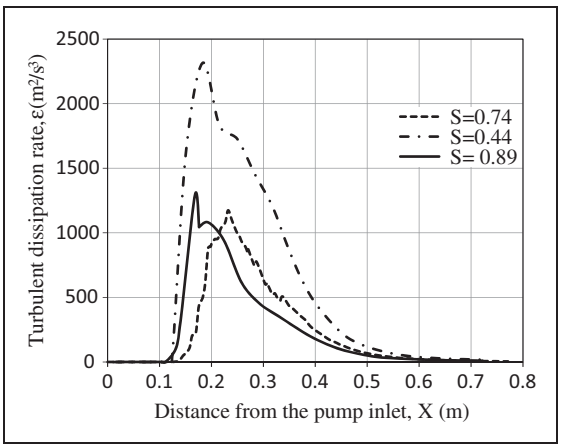

Figure 8. Dissipation rates of the turbulent kinetic energy along the jet pump centerline for the driving nozzle positions at optimum flow ratios ($A = 7.94$ and $L = 7.4$).

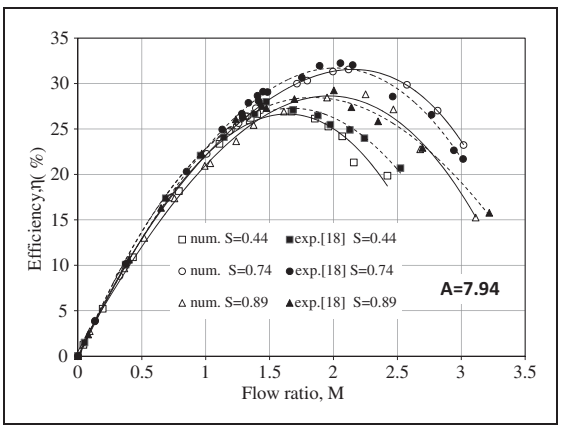

Figure 7. Effect of driving nozzle position on the efficiency of the pump.

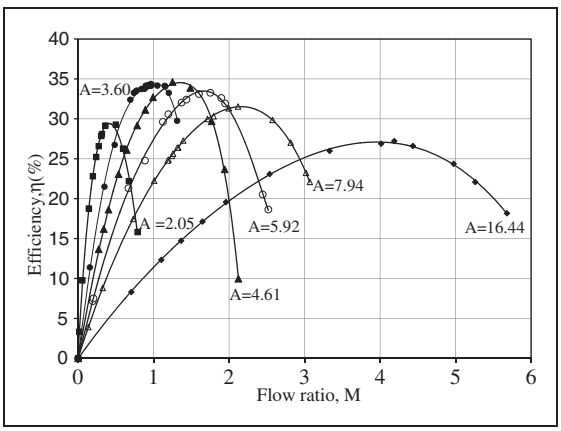

Figure 9. Numerical efficiency curves at various area ratios.

ratio means a lower flow rate ratio. In other words, the efficient-operating range for higher area ratios is larger.

The pressure ratios, mass flow ratios, and the numerical and experimental efficiencies at optimum operating conditions for the area ratios used in the current study together with the deviations in efficiency are listed in Table 3. According to this table, a maximum numerical efficiency of 34.6% is obtained at $A = 4.61$ and $M = 1.24$. The percentage of variation in the numerical optimum efficiency in the area ratio range between 4.61 and 16.44 is a high ratio of approximately 21.4%. Considering the uses of water jet pumps, higher area ratios are required when a smaller pump head or higher suction flow rates are needed and conversely, when a larger pump head is required, then lower area ratios are needed. As seen in Table 3, the numerical and experimental pressure ratios are equal this is because, as mentioned above, the pressure inlet and outlet boundary conditions for the computation domain are the same as those in the experimental study that was used for comparison. According to Table 3, the highest deviation from optimum experimental efficiency is 10.4% at an area ratio of 2.04 and the average deviation according to all area ratios is 4.4%.

Optimum design curves

The curve drawn through the peak points of the efficiency curves for the constant area ratio shows the optimum efficiency of the water jet pump. For being more illustrative, using the data from Table 3, the optimum numerical and experimental performance curves plotted on the graph shown in Figure 10.

The trends of the optimum pressure ratio and the efficiency curves depending on the flow ratio are similar to those of the curves drawn for only an area ratio. Namely, the optimum efficiency first suddenly increases and then slowly decreases, while pressure ratio always decreases with the mass flow ratio.

In order to obtain the best efficiency from the water jet pump in each area ratio, the tested pumps were designed so that the centerlines of the driving nozzle and the jet pump body (consisting of a suction nozzle, mixing chamber and diffuser) coincide. In addition to this, the entrained fluid was provided to flow in an axisymmetrical path into the mixing chamber through the suction nozzle from the suction chamber.

When considering the efficiency, the maximum difference of 3.4% between the authors' numerical results and experimental results available in Ref. 18 at the area ratio $A = 2.04$ corresponds to a highest deviation of 10.4% in percentage terms. In addition, in order to make a comparison with other researchers' experimental data in Ref. 19, two additional curves are also plotted in Figure 10. Experimental efficiency results determined by Shulz and Fasol are always greater than the authors' numerical and experimental efficiencies. There is a good agreement between pressure ratios. Shulz and Fasol carried out their experiments using large-scale jet pumps. Reynolds number based on the mixing tube diameter d_m was $Re_m = 1.1 \times 10^6 \pm 30\%$. In this study, small-scale jet pumps with a geometric scale ratio of around 1/3 were used in both numerical and experimental tests and Reynolds number had a smaller value ($Re_m = 3.16 \times 10^5 \pm 7.2\%$). Scale effect is the main reason for the increase of efficiency in large-scale jet pumps. Maximum deviation of the efficiency obtained by Shulz and Fasol from the numerical efficiency is 11.3% at the flow ratio $M \cong 2$.

Consequently, we can say that the CFD simulation results are in good agreement with the experimental data in the optimum operating conditions. According

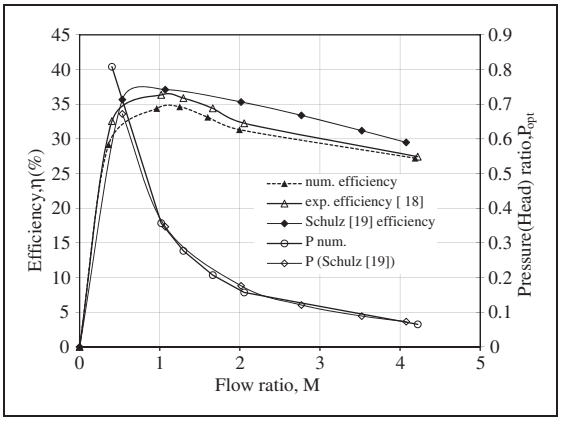

Figure 10. The numerical and experimental optimum curves.

Table 3. Deviations in efficiency at optimum operating conditions.

A	$P_{num.} = P_{exp}$	M_{num}	M_{exp} [18]	η_{num} (%)	η_{exp} (%) [18]	Deviations in η (%)
2.05	0.808	0.37	0.40	29.1	32.5	10.4
3.60	0.357	1.00	1.02	34.3	36.3	5.3
4.61	0.277	1.25	1.29	34.6	35.8	3.4
5.92	0.207	1.60	1.66	33.1	34.4	3.7
7.94	0.157	2.03	2.05	31.3	32.2	2.8
16.44	0.065	4.17	4.22	27.2	27.4	0.8

to the optimized results obtained over a wide range of area ratios, the numerical CFD data calculated using the three-dimensional transition SST turbulence model were validated with experimental data. Based on this conclusion and making use of the data in Table 3, the numerical optimum design curves are plotted in Figures 11 and 12.

The curves of the pressure and area ratio at the maximum efficiencies are also optimum curves. The characteristic curves indicating the optimum operating conditions in Figure 11 are the main optimum design curves required to be used in the dimensioning of the water jet pumps. P_{opt} and M_{opt} specified in this figure are the optimum flow parameters, whereas A_{opt} is optimum geometrical parameter. When one of these dimensionless parameters is selected in the design stage for a jet pump, the other two dimensionless parameters are determined from these graphs. If other parameters are arbitrarily chosen for a given parameter, the pump may operate with a lower efficiency or in the cavitation-region making a noise, and it may not even perform its function.

Figure 12 indicates the variation of the optimum relative nozzle position S_{opt} and the optimum relative mixing length L_{opt} depending on the area ratio. These graphs are plotted based on the results of numerical sensitivity tests mentioned in section "Effects of geometrical parameters on the performance of jet pump." As seen from Figure 12, the value of the relative nozzle position always decreases with the increase of the area ratio. However, the relative length L_{opt} sharply rises from first value up to $A_{opt} \cong 4$ and then remains constant at a value of 7.4 for $A_{opt} > 4$. For example, if the flow ratio is selected as $M = 2$, the optimum area and pressure ratio are found to be $A_{opt} = 8$ and $P_{opt} = 0.16$, respectively, from Figure 11. The optimum relative mixing chamber and nozzle position for this area ratio are determined to be $L_{opt} = 7.4$ and $S_{opt} = 0.74$ from Figure 12. According to Figure 10, the efficiency at the optimum operating point will be approximately 32%.

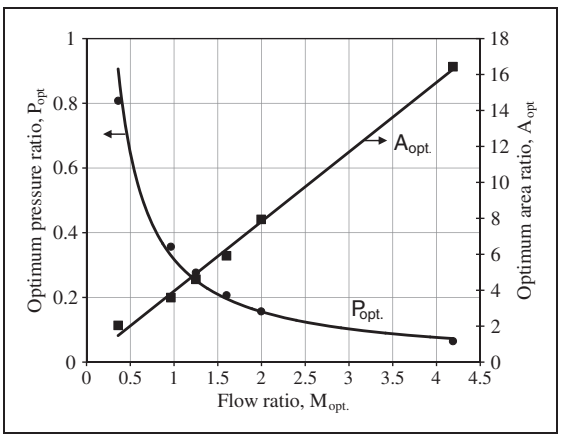

Figure 11. Optimum design curves.

Assessment of cavitation resistance

In this numerical optimization study, non-cavitating performance of water jet pumps is investigated at previously specified operating conditions. Cavitation in these pumps results from high driving pressure and it does not significantly affect the performance of the jet pump until a given net positive suction head of secondary fluid. A few cavitation prediction parameters commonly used in the literature exist.[19,25,26] In order to determine the cavitation resistance of the analyzed jet pumps, the cavitation number defined as follows in Ref. 19 will be used

$$\sigma = \frac{p_{s,t}}{p_{p,t} - p_{s,t}}; \quad p_{i,t} = p_{i,absolute} + \frac{\rho V_i^2}{2};$$
$$p_{i,absolute} = p_{gage} + p_{atm} \tag{23}$$

Critical cavitation number σ_{cr} represents the cavitation number at which the cavitation starts in the jet pump, that is, vapor bubbles appear at the jet boundary. This incipient cavitation does not reduce the efficiency of the jet pump. If the intensity of cavitation increases and the bubbles spread to wall of mixing

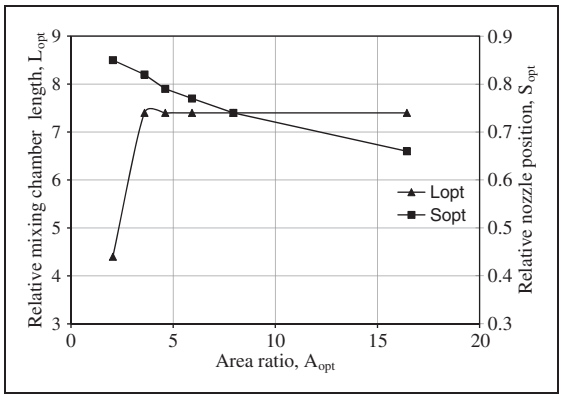

Figure 12. Optimum relative nozzle position S_{opt} and mixing chamber length L_{opt}.

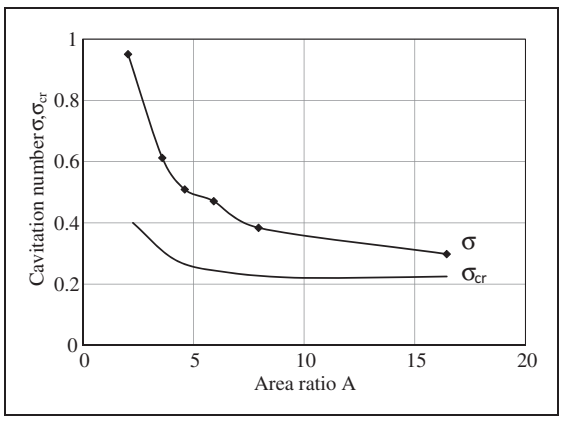

Figure 13. Cavitation numbers at the optimum operating conditions.

tube, then the efficiency drops rapidly. Figure 13 shows the cavitation numbers σ and σ_{cr} as a function of the area ratio. The critical cavitation number σ_{cr} is an experimental number and taken from Ref 19. σ is computed from equation (23) using the boundary conditions of the jet pump. According to graphs in this figure, σ is always greater than σ_{cr} and thus the whole of the operating range is in the non-cavitating region. However, as the area ratio increases, the difference between these cavitation numbers gradually decreases and hence operating conditions approach the cavitating region.

Conclusion

In the flow simulation study, the optimization of six different water jet pumps having area ratios in the range of 2.05–16.44 was carried out using the transition SST turbulence model. For the purpose of validation, the numerical results of the optimization work were compared with the optimized experimental data with the same boundary conditions in the literature. At the optimum operating conditions, the deviations of numerical results relative to the experimental results remained approximately within a range of 10% for the efficiency of the similar water jet pump. Thus, the CFD simulation results obtained by the transition SST model were validated. Although the transition SST turbulence model generally slightly underestimates the optimum efficiency, it provides detailed insight into geometrical effects in the water jet pumps.

The optimum numerical design curves generated in the study can be used in designs of water jet pumps. The highest efficiency of 34.6% determined by the ***γ-Re_θ model*** was obtained for the area ratio of 4.61, flow ratio of 1.24, and pressure ratio of 0.277. It is concluded that the physics of flow within liquid jet pumps can be analyzed in detail with numerical simulation and the possibilities/methods to improve their performance can be determined. Furthermore, optimization can be easily performed by using the CFD technique, provided that efficient and accurate turbulence models are validated with experimental tests.

Funding

This research was supported by Selçuk University under the BAP Project No: 11201037.

References

1. Prakeao C, Takayama S, Aoki K, et al. Numerical prediction on optimum mixing throat length for drive nozzle position of the central jet pump. In: *10th international symposium on flow visualization*, Japan, 26–29 August 2002.
2. Hayek MD and Hammoud AH. Prediction of liquid jet pump performance using computational fluid dynamics. In: *Proceedings of the 4th WSEAS international conference on fluid mechanics and aerodynamics*, Elounda, Greece, 21–23 August 2006, pp.148–153.
3. Long X, Han N and Chen Q. Influence of nozzle exit tip thickness on the performance and flow field of jet pump. *J Mech Sci Technol* 2008; 22: 1959–1965.
4. Narabayashi T, Yamazaki Y and Kobayashi H. Flow analysis for single and multi-nozzle jet pump. *JSME Int J Ser B* 2006; 49: 933–940.
5. Li C and Li YZ. Investigation of entrainment behavior and characteristics of gas–liquid ejectors based on CFD simulation. *Chem Eng Sci* 2011; 66: 405–416.
6. Utomo T, Jin Z, Rahman MS, et al. Investigation on hydrodynamics and mass transfer characteristics of a gas-liquid ejector using three-dimensional CFD modeling. *J Mech Sci Technol* 2008; 22: 1821–1829.
7. Kandakure MT, Gaikar VG and Patwardhan AW. Hydrodynamic aspects of ejectors. *Chem Eng Sci* 2005; 60: 6391–6402.
8. Yuan G, Zhang L and Zhang H. Numerical and experimental investigation of performance of the liquid–gas and liquid jet pumps in desalination systems. *Desalination* 2011; 276: 89–95.
9. Fan J, Eves J, Thompson, et al. A computational fluid dynamic analysis and design optimization of jet pumps. *Comput Fluids* 2011; 46: 212–217.
10. Hemidi A, Henry F, Leclaire S, et al. CFD analysis of a supersonic air ejector. *Part I: Experimental validation of single-phase and two-phase operation*. Appl Therm Eng 2009; 29: 1523–1531.
11. Varga S, Oliveira AC and Diaconu B. Numerical assessment of steam ejector efficiencies using CFD. *Int J Refrig* 2009; 32: 1203–1211.
12. Pianthong K, Seehanam W, Behnia M, et al. Investigation and improvement of ejector refrigeration system using computational fluid dynamics technique. *Energ Convers Manage* 2007; 48: 2556–2564.
13. Winoto SH, Li H and Shah DA. Efficiency of jet pumps. *J Hydraul Eng* 2000; 126: 150–156.
14. Neto IEL and Porto RM. Performance of low-cost ejectors. *J Irrig Drain Eng* 2004; 130: 122–128.
15. Henzler HJ. Design of ejectors for single-phase material systems. *Ger Chem Eng* 1983; 6: 292–300.
16. Hammoud AH. Effect of design and operational parameters on jet pump performance. In: *Proceedings of the 4th WSEAS international conference on fluid mechanics and aerodynamics*, Elounda, Greece, 21–23 August 2006, pp.245–252.
17. Karambirov SN and Chebaevskii VF. Possibilities of improving ejector pump characteristics. *Chem Petrol Eng* 2005; 41: 1–2.
18. Yapıcı R. Determination of optimum operating conditions of water-jet pumps. PhD Thesis, Selçuk University, Turkey, 1990 [in Turkish].
19. Schulz F and Fasol KH. *Wasserstrablpumped zur Förderung von Flüssigkeiter*. Wien: Springer-Verlag, 1958.
20. El Gazzar M, Meakhail T and Mikhail S. Experimental study of the effect of drag reduction agents on the performance of jet pump. *Proc IMechE, Part A: J Power and Energy* 2006; 220: 379–386.
21. El Gazzar M, Meakhail T and Mikhail S. Numerical and experimental study of the influence of drag reduction agent (carboxy methyl cellulose) on the central jet pump performance. *Proc IMechE, Part A: J Power and Energy* 2007; 221: 1067–1073.

22. ANSYS, Inc. *Theory guide ANSYS FLUENT 14.0*. Canonsburg, PA: ANSYS, Inc, 2009.
23. Langtry RB and Menter FR. Transition modeling for general CFD applications in aeronautics. AIAA Paper 2005-0522, 2005.
24. Menter FR, Langtry RB, Likki SR, et al. Correlation-based transition model using local variables part I – model formulation. *J Turbomach* 2006; 128: 413–422.
25. Sanger NL. An experimental investigation of several low area-ratio water jet pumps. *ASME J Basic Eng* 1970; 92: 11–20.
26. Neto IEL. Maximum suction lift of water jet pumps. *J Mech Sci Technol* 2011; 25: 391–394.

Appendix

Notation

a	cross-sectional area (m^2)
A	area ratio $= a_m/a_n$, (area of mixing chamber to exit area of nozzle)
d	diameter (m)
k	turbulent kinetic energy (m^2/s^2)
l	length (m)
L	relative length of mixing chamber
$\dot{m}$	mass flow rate (kg/s)
M	flow rate ratio
P	static pressure (kPa)
P	pressure (head) ratio
Re	Reynolds number
s	driving nozzle position (m)
S	relative position of driving nozzle, strain rate magnitude (s^{-1})
T_i	turbulence intensity (%)
u_i	velocity component (m/s)
x_i	space coordinate (m)
X	distance from the jet pump inlet (m)

Greek letters

δ	boundary layer thickness (m)
ε	dissipation rate of the turbulent kinetic energy (m^2/s^3)
η	jet pump efficiency
μ	dynamic viscosity (Pa·s)
μ_t	turbulent viscosity (Pa·s)
θ	momentum thickness (m)
ρ	fluid density (kg/m^3)
ω	specific dissipation rate (s^{-1})
Ω	vorticity magnitude (s^{-1})

Subscripts

d	diffuser outlet
exp	experimental
m	mixing chamber/tube
n	driving nozzle outlet
num	numerical
opt	optimum
p	driving (primary) nozzle inlet
s	suction (secondary) nozzle inlet
t	total, transition
υ	vorticity